Interlink between abnormal water imbibition in hydrophilic and rapid flow in hydrophobic nanochannels

Interlink between abnormal water imbibition in hydrophilic and rapid flow in hydrophobic nanochannels

Runfeng Zhou[1], Mehdi Neek-Amal[2,3], Francois M. Peeters[3,4], Bofeng Bai[1], and Chengzhen Sun[1*]
[1] *State Key Laboratory of Multiphase Flow in Power Engineering, Xi'an Jiaotong University, Xi'an, Shaanxi 710049, China*
[2] *Department of Physics, Shahid Rajaee Teacher Training University, 16875-163 Lavizan, Tehran, Iran*
[3] *Departement Fysica, Universiteit Antwerpen, Groenenborgerlaan 171, B-2020 Antwerpen, Belgium*
[4] *Departamento de Física, Universidade Federal do Ceará, Fortaleza-CE 60455-760, Brazil*

A multiscale approach, involving the refinement of the Lucas-Washburn model, a detailed analysis of recent experimental data, and extensive molecular dynamics simulations, is employed to investigate rapid water flow and water imbibition within nanocapillaries. Through a comparative analysis of capillary rise in hydrophilic nanochannels, an unexpected reversal of the anticipated trend, with an abnormal peak, of imbibition length below the size of 3 nm was discovered in hydrophilic nanochannels, surprisingly sharing the same physical origin as the well-known peak observed in flow rate within hydrophobic nanochannels. The extended imbibition model is applicable across diverse spatio-temporal scales and validated against simulation results and existing experimental data for both hydrophilic and hydrophobic nanochannels. This surprising direct interlink between water imbibition in hydrophilic and rapid flow in hydrophobic nanochannels provides unified insights into nanofluidic dynamics, marking an essential step forward in this field.

Introduction.—The phenomenon of spontaneous water flow involves the migration of water into nanochannels (NCs) driven by capillary forces. In recent years, this phenomenon has garnered significant attention, driven by both fundamental physics and potential applications [1]. Recent reports have explored water transport through hydrophilic (HPI) and hydrophobic (HPO) NCs, spanning confinement heights from a single atomic layer ($\approx$ 0.34 nm) to several dozen atomic planes ($\sim$10 nm)[2–15]. The first set of studies focused on measuring fluid weight loss due to evaporation, primarily water [1–3], while the second set of experiments concentrated on the time-dependent position of the meniscus [6–8].

However, as the characteristic length of the flow domain decreases to the nanoscale and below, the predictive power of conventional theories governing water flow, such as the Hagen-Poiseuille (H-P) theory [16], and imbibition flow, represented by the Lucas-Washburn (LW) equation ($x_{\rm LW} = \sqrt{\frac{h\gamma\cos\theta_{\rm e}}{3\mu}t} = \sqrt{2\mathcal{D}_{\rm LW}t}$ where $x_{\rm LW}$ is the imbibition length, t is the imbibition time, γ is the surface tension, $\theta_{\rm e}$ is the equilibrium contact angle, μ is the viscosity and $\mathcal{D}_{\rm LW} \equiv \frac{h\gamma\cos\theta_{\rm e}}{6\mu}$ is a defined characteristic transport coefficient which has the units of diffusion coefficient, hereafter referred to as the imbibition coefficient) [6, 7], reaches its limitations. An accurate description of water flow and spontaneous imbibition at the nanoscale remains a formidable challenge [16–19]. For example, a notable departure from the predictions of aforementioned classical theories regarding both imbibition length and water weight loss rate becomes increasingly pronounced as the confinement size decreases. This trend is evident in various sets of experimental data, as one typical demonstrated for HPI channels in Fig. 1. The shaded area signifies the range of NC heights where experimental data is notably scarce, especially below 10 nm. Furthermore, a sequence of studies concentrating on water transport through HPO graphene NCs and carbon nanotubes has underscored the substantial influence of disjoining pressure in confined, narrow channels, highlighting the constraints of classical H-P equations [2, 16, 19]. Particularly, in situations where channels have a restricted capacity for water layers, this phenomenon is traditionally referred to as "rapid water flow through nanocapillaries" [2, 4, 20, 21]. The observed deviation can be attributed to a myriad of factors, each contributing to in-

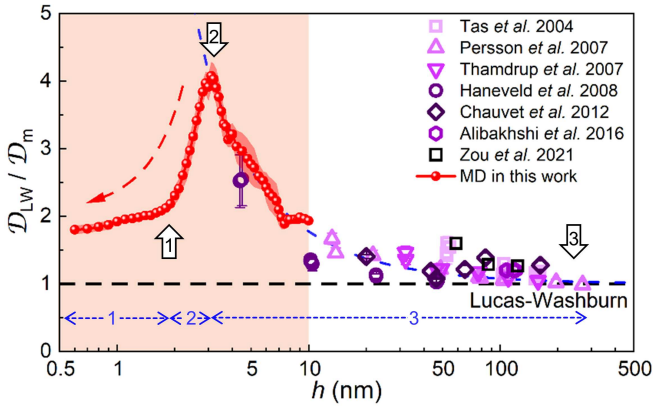

FIG. 1. Deviations in the ratio between the traditional LW equation (black dashed horizontal line) at various channel heights for both experimental and MD data of HPI NCs. The blue dashed line represents the exponential deviation from the classical limit, becoming particularly evident starting from 300 nm and extending down to around and below 10 nm. The red dashed arrow serves as a guide to the eye, emphasizing the deviation from the classical prediction below 3 nm. The arrows indicate distinct regimes.

* sun-cz@xjtu.edu.cn

tricate and significant nanoconfinement effects on fluids [5–8, 11].

In this Letter, we present a refined version of the LW equation aimed at elucidating a diverse range of experimental observations in both frictional loss and frictionless NCs, including recent findings on water flow and imbibition [4]. This adaptation, validated through extensive molecular dynamics (MD) simulations on HPI silica NCs (0.6-10 nm in height) and informed by previous MD work on HPO graphene NCs [2, 22], incorporates crucial factors such as enhanced viscosity and disjoining pressure. Our analysis of HPI NCs has significantly influenced our approach to the study of HPO NCs, prompting a reexamination of the longstanding puzzle posed by rapid water flow through HPO NCs.

We systematically compare our modified Lucas-Washburn (MLW) equation with diverse experimental data obtained from both HPI and HPO NCs. The primary objective is to establish a direct correlation between these observations, thereby extending the applicability of the LW equation to various NC types. The H-P equation serves to model viscous flow in channels, incorporating parameters such as viscosity, pressure gradient, and channel dimensions. In contrast, the LW equation characterizes capillary imbibition, relying on factors like viscosity, contact angle, and channel geometry. It's noteworthy that both models emerge as consequences of the Navier-Stokes equation.

The model and method.—Our non-equlibrium MD simulations are carried out using LAMMPS [23, 24], within a simulation box measuring $L_x \times L_y = 75\,\text{nm} \times 2.5\,\text{nm}$. The dimensions of the box are adjusted to accommodate the varying NC heights (h), ranging from 0.6 nm to 10 nm. The NCs are constructed from hydroxylated silica layers with dimensions $d_x \times d_y \times d_z = 34\,\text{nm} \times 2.5\,\text{nm} \times 1.6\,\text{nm}$, separated by h, as illustrated in the inset of Fig. 2(a). Silica layers are obtained by cleaving α-quartz crystal planes (001), ensuring HPI conditions. The simulation uses the consistent valence force field (CVFF) [25] for silica NCs and the SPC/Fw model for water molecules. Interactions are represented using the 12-6 Lennard-Jones potential with Coulombic interactions and a cutoff distance of 1 nm. Periodic boundaries, a time step of 1 fs, and temperature control at 300 K using the Nosé-Hoover thermostat are applied. Initial equilibration includes a nonvisual force wall between the NC entrance and bulk water for 5 ns, followed by a 10 ns trajectory sampling simulation (more details in Supporting Information (SI) section SI-I).

The determination of imbibition length in NCs requires discretization of the water domain, computation of water density, interface identification, and meniscus shape determination. The typical imbibition length, denoted as $x(t)$ and defined as the distance between the NC entrance and the bottom of the meniscus curve, is illustrated in the inset of Fig. 2(a) (more details can be found in SI-II).

Deviation from the LW equation in frictional loss NCs.—In Fig. 2(a) (and Fig. S3), we depict the

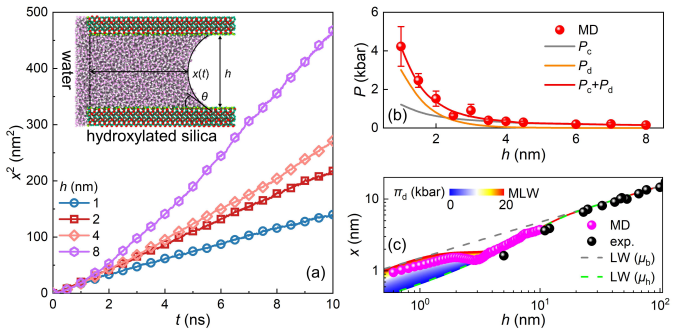

FIG. 2. (a) Temporal evolution of the square of the imbibition length, x^2. Inset: Side view of the water imbibition meniscus in the MD simulation setup, represented by the black curve. (b) Different type of driving pressures as a function of height. (c) Influence of the disjoining pressure parameter (π_d) on the imbibition length of water in HPI silica nanochannels.

MD data for the temporal evolution of the square of the imbibition length, $x^2(t)$, within hydroxylated silica NCs of varying heights. Notably, in wider NCs, $x^2(t)$ exhibits a subtle deviation from the linear relationship during the initial stages. This initial deviation can be primarily attributed to three key factors: the inertia effect [26], the dynamic contact angle (DCA) effect [27] and entrance effect[28, 29]. While the inertia effect tends to rapidly diminish within tens of picoseconds [30], the more prolonged deviation predominantly results from the DCA and the entrance effect. The presence of a non-linear relationship during the initial stages suggests that factors beyond viscosity may significantly influence nanoscale imbibition dynamics.

Significantly, in narrower NCs, the measured imbibition coefficient ($\mathcal{D}_\text{m}$) as well as the imbibition length (x) closely conforms to LW predictions, as evident from the curved red dashed arrow in Fig. 1. This intriguing outcome contradicts the expected trend based on previous experimental data in Fig. 1 [6–8, 10–15], where deviations in $\frac{\mathcal{D}_\text{LW}}{\mathcal{D}_\text{m}}$ were anticipated to increase as channel height decreased, as indicated by the blue dashed line in Fig. 1. Comparing our simulation results with existing experimental data, we conclude that the deviation in imbibition coefficient and the corresponding imbibition length exhibits a non-monotonic variation with h.

The ratio between $\mathcal{D}_\text{LW}$ from original LW equation and $\mathcal{D}_\text{m}$ from MD data presented in Fig. 1 highlights the complex nature of water transport in silica NCs, particularly when h is below 10 nm. The existing experimental data within this h range is limited, with only sparse information around $h = 5$ nm, posing challenges for drawing definitive conclusions. Technical constraints in measuring imbibition length for channels below 10 nm further compound the issue, underscoring the necessity for additional experimental and MD data to facilitate accurate comparisons.

To analyze the height scales comprehensively, we cat-

egorize them into four distinct ranges: i) $h < 2\,\text{nm}$, ii) $2 < h < 3\,\text{nm}$, iii) $3 < h < 300\,\text{nm}$, and iv) $h > 300\,\text{nm}$. In the last segment, nanoscale effects can be disregarded and the LW equation works well. In the other ranges, the confinement effect becomes prominent and leads to an increase in effective viscosity, and significant deviations are observed, with a profound peak around 3 nm. Below this, the short-range disjoining pressure becomes prominent and enhances imbibition while compensating for nanoscale flow, and a rapid decrease in deviation is evident until 2 nm, where the compensation effect of disjoining pressure on viscosity weakens and a slower decrease is observed (see below).

Modified LW equation.—In alignment with our approach for HPO NCs [16], we introduce modifications to the LW equation. These modifications incorporate an effective viscosity term [31], denoted as μ_h, which varies with h. This approach diverges from conventional bulk viscosity, denoted as μ_b, and is defined as follows: $\mu_h = \mu_\text{b}(1 + \mu_0 e^{-h/\lambda})$. Here, μ_0 and λ are characteristic parameters [4, 16], and $\mu_\text{b} = 0.89$ mPa·s represents the viscosity of bulk water at room temperature (more details in SI-III).

Additionally, while taking into account Laplace's pressure and the viscous pressure drop within the NCs, we introduce the disjoining pressure (P_d) [2, 16] which is the pressure difference between the water inside the NC and outside the channel. Therefore, the total driving pressure for liquid flow can be approximated as $P = P_\text{c} + P_\text{d}$, where $P_\text{c} = \frac{2\gamma\cos\theta_\text{e}}{h}$ represents the capillary pressure in the classical regime. It's worth noting that P_d characterizes the water-surface interaction, which can dominate at the nanoscale but decreases rapidly with increasing h. We can express it as $P_\text{d} \approx \pi_\text{d} e^{-h/\lambda'}$ (more details in SI-IV) as illustrated in Figs. 2(b,c) for HPI NCs, while for HPO NCs, it was studied in Ref. [2, 16] (see Fig. S7 with more details in SI-VII).

In addition to the aforementioned corrections for viscosity and disjoining pressure, we further extend the LW equation, we multiply pressure by $1+\frac{6\delta}{h}$, which takes into account the well-known slip term [32–36]. Here, δ represents the slip length, which can be negligible (small) for HPI silica (hexagonal boron nitride, hBN) NCs. Consequently, the LW equation can be approximated for long times ($t \gg 1\ \mu$s) as follows:

$$x_\text{MLW} \approx \sqrt{\frac{h^2}{6}\frac{P}{\mu_h}\left(1+\frac{6\delta}{h}\right)t}. \tag{1}$$

Under these conditions, Eq. (1) converges to the original LW equation for microchannels, aligning with experimental observations. However, for NCs, adjustments to $\mathcal{D}$ (that is, P and μ) are necessary. Further insights, a complete form of the modified LW equation and a detailed analysis of the long-time approximation of Eq. (1) can be found in SI-VI. A comprehensive list of various modifications to LW equation can be found in the literature[18, 29, 37]. By incorporating parameters derived from our/others MD simulations (Table I), we achieve close agreement between the predicted imbibition length and MD and experimental results in both narrow and wide channels. For instance, in Fig. 2(c) (and Fig. S7(b)), we illustrate the impact of varying π_d in Eq. (1) within the range 0-20 kbar (with the provided parameters in Table I) to explain the non-monotonic deviation in imbibition length. The appearance of disjoining pressure compensates the large deviation resulting from the enhanced viscosity (more details in SI-III and SI-IV).

In this Letter, the parameters for refining the LW equation were determined based on MD simulation data from silica, as well as previous simulations on graphene and hBN [2, 16, 22]. The results indicate a narrow parameter range around the values obtained from MD simulations, as shown in Table I. For example, contact angles for silica, graphene, and hBN are approximately 15°, 89.95°, and 89°, respectively, and the π_d values are a few kilo-bar, aligning with established values. It is crucial to note that these parameters fall within the expected range. Given the broad spectrum of h and time scales considered in our study, demanding highly precise parameter values exceeds the bounds of physical intuition.

TABLE I. The parameters employed in MLW model for different NCs. Parameters for graphene are derived from both our current and previous studies[2, 16, 22]

channel	θ_e (°)	μ_0	λ (nm)	π_d (kbar)	λ' (nm)
Graphene	89.5-90	~ 1000	0.1-0.6[16]	~ 3[2]	~ 0.5
hBN	86.5-89.5	~ 4.8	~ 4	~ 5	~ 0.36
Silica	0-60	4.8	4.1	11.37	0.72

Modified LW model for experimental data of water flow through HPI/HPO NCs.—We consolidate the reliability of our model (Eq. (1) by conducting a comprehensive examination of experimental data from the literature. This analysis includes studies on water imbibition into silica NCs [6–8, 10, 11, 14], as well as hBN NCs [4]. Figure 3(a) provides a comprehensive comparative analysis of our MD results (magenta dots) with theoretical predictions from the original (grey dashed line) and modified LW equations using parameters from the third row of Table I and $\delta = 0$ nm for silica (color spectrum), showing close agreement between experimental data (exp.), MD and MLW for heights from 0.6 nm to 1 μm and contact angles represented by color bars within the range of 0-60°. While elements of our modification can be found in existing literature, our work's significance lies in uniting studies on HPO and HPI NCs.

Next, we delve into the experimental aspect of our study, where we integrate experimental measurements and link them with both MLW and MD methods. The aim is to transform weight loss rate data, widely used in recent experiments [2, 4], into imbibition length data. This breakthrough not only fills a crucial gap in nanofluidic research but also lays the foundation for a theoretical framework that could revolutionize nanofluidic mea-

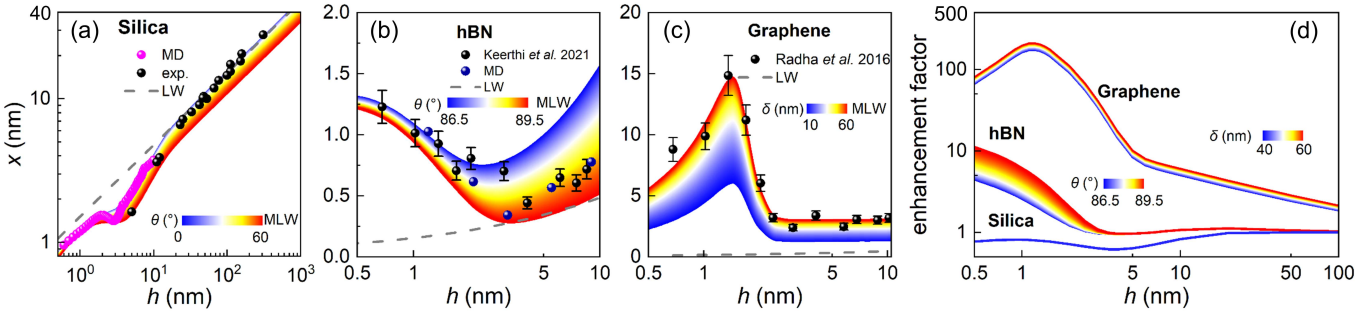

FIG. 3. The imbibition lengths for silica (a) and hBN (b), determined by x_{MLW}, vary with contact angles within the range of 0-60 degrees for silica and 86.5-89.5 degrees for hBN (indicated by color bars), respectively. Panel (c) shows the imbibition length variations for graphene with different slip lengths within the range of 10-60 nm. Experimental data obtained from various literature sources, as explained in the main text, is represented by dots. The dashed grey lines represent the results of the original LW equation. (d) The variation of enhancement factor ($\epsilon = \frac{x_{\mathrm{MLW}}}{x_{\mathrm{LW}}}$) with the channel height.

surements. The weight loss rate data, represented as $Q = \rho w h V$, where ρ, w denoting the denisty and channel width and V the streamline velocity in a channel with length L, can be related to imbibition length data through imbibition velocity $\frac{\mathrm{d}x}{\mathrm{d}t}|_{x=L} = \frac{\mathcal{D}}{L}$ using the defined imbibition coefficient $\mathcal{D} = \frac{x^2}{2t}$, where

$$V|_{x=L} = \frac{Q}{\rho w h} = \frac{\mathcal{D}}{L}. \tag{2}$$

By determining the value of $\mathcal{D}$, one is able to calculate experimental values of $x = \sqrt{2\frac{QL}{\rho w h}t}$.

In Figs. 3(b) and 3(c), we made the conversion of weight loss data obtained from hBN and graphene NCs. We used $\delta = 1\,\mathrm{nm}$ to represent hBN and $\delta = 60\,\mathrm{nm}$ for graphene, which are values extracted from Ref. [4]. The colored spectrum elegantly depicts the results of x_{MLW}, showing exceptional agreement with experimental observations (black dots). For comparison, additional MD simulations give imbibition results in the hBN NCs (navy dots in Fig. 3(b) with a shift), showing agreement with experiment and proposed MLW model. These results were obtained using the parameters provided in Table I, primarily derived from MD simulations. Notably, for both hBN and graphene, contact angles close to 90° yield excellent agreement. The differences observed between graphene and hBN, as indicated by the varying δ values, stem from the distinct water adsorption behaviors in HPI channels. Specifically, from Fig. 3(b), it is evident that the contact angles should be close to 90° even for large h in hBN NCs. Additionally, Fig. 3(c) illustrates that $\delta =$ 60 nm in graphene NCs results in excellent agreement with experiments for $h <$ 2-3 nm. However, beyond this range of heights, no significant effects are observed.

Eventually, we calculate the water imbibition enhancement factor, denoted as $\epsilon = \frac{x_{\mathrm{MLW}}}{x_{\mathrm{LW}}}$. The enhancement of flow has been extensively documented in studies involving water transport through carbon nanotubes [38–41]. In Fig. 3(d), we present the variation of ϵ with h. Remarkably, a substantial two-orders-of-magnitude reduction in ϵ is observed from graphene (with $\theta = 89.95°$) to hBN (with $\theta = 89°$) at $h \approx 1.4$ nm. Even with this reduction, hBN demonstrates significantly faster flow compared to silica. This notable decrease in ϵ between graphene and hBN is consistent with experimental findings in weight loss measurements [4], underscoring a profound interlink between weight loss measurements and imbibition length identification. We term this intricate relationship as the "interlink" between these phenomena, revealing a previously unexplored facet of nanofluidic dynamics. Moreover, in silica, when the height $h <$ 50 nm, we observed a decrease in ϵ (where $\epsilon < 1$) due to enhanced viscosity. Notably, as the height h decreases to 2-3 nm, the enhancement factor rises owing to the emergence of disjoining pressure. Moreover, we can extend this approach to nanotubes with radius denoted as r by adapting the LW equation as follows: $x_{\mathrm{MLW}} \approx \sqrt{\frac{Pr^2}{4\mu_r}\left(1 + \frac{4\delta}{r}\right)t}$, where P and μ_r represent radius-dependent pressure and viscosity, respectively.

In summary, we presented a generalization of the LW equation that included enhanced viscosity, disjoining pressure, and slip conditions in both HPO and HPI NCs. Our model is valid over spatial scales from nanometers to hundreds of nanometers and temporal scales spanning from nanoseconds to hours. Thus, our model provides a unified framework for comprehending and predicting the spontaneous imbibition of fluids within channels. This modified equation was rigorously validated against MD results and existing experimental data, accurately forecast imbibition dynamics within NCs. Notably, our model effectively addresses wall slip effects, particularly in graphene NCs.

Acknowledgment. We gratefully acknowledge the financial support provided by the National Natural Science Foundation of China (Project No. 51888103, 52222606). Part of this project was supported by the Flemish Science Foundations (FWO-Vl) and the Iranian National Science Foundation.

[1] Y. You, A. Ismail, G.-H. Nam, S. Goutham, A. Keerthi, and B. Radha, Annual Review of Materials Research **52**, 189 (2022).

[2] B. Radha, A. Esfandiar, F. Wang, A. Rooney, K. Gopinadhan, A. Keerthi, A. Mishchenko, A. Janardanan, P. Blake, L. Fumagalli, *et al.*, Nature **538**, 222 (2016).

[3] S. Goutham, A. Keerthi, A. Ismail, A. Bhardwaj, H. Jalali, Y. You, Y. Li, N. Hassani, H. Peng, M. V. S. Martins, *et al.*, Nature Nanotechnology **18**, 596 (2023).

[4] A. Keerthi, S. Goutham, Y. You, P. Iamprasertkun, R. A. Dryfe, A. K. Geim, and B. Radha, Nature Communications **12**, 3092 (2021).

[5] Q. Xie, M. A. Alibakhshi, S. Jiao, Z. Xu, M. Hempel, J. Kong, H. G. Park, and C. Duan, Nature Nanotechnology **13**, 238 (2018).

[6] N. R. Tas, J. Haneveld, H. V. Jansen, M. Elwenspoek, and A. van den Berg, Applied Physics Letters **85**, 3274 (2004).

[7] F. Persson, L. H. Thamdrup, M. B. L. Mikkelsen, S. Jaarlgard, P. Skafte-Pedersen, H. Bruus, and A. Kristensen, Nanotechnology **18**, 245301 (2007).

[8] L. H. Thamdrup, F. Persson, H. Bruus, A. Kristensen, and H. Flyvbjerg, Applied Physics Letters **91**, 163505 (2007).

[9] K. M. van Delft, J. C. Eijkel, D. Mijatovic, T. S. Druzhinina, H. Rathgen, N. R. Tas, A. van den Berg, and F. Mugele, Nano Letters **7**, 345 (2007).

[10] J. Haneveld, N. R. Tas, N. Brunets, H. V. Jansen, and M. Elwenspoek, Journal of Applied Physics **104**, 014309 (2008).

[11] N. A. Mortensen and A. Kristensen, Applied Physics Letters **92**, 063110 (2008).

[12] S. Gruener, T. Hofmann, D. Wallacher, A. V. Kityk, and P. Huber, Physical Review E **79**, 067301 (2009).

[13] J. W. Van Honschoten, N. Brunets, and N. R. Tas, Chemical Society Reviews **39**, 1096 (2010).

[14] F. Chauvet, S. Geoffroy, A. Hamoumi, M. Prat, and P. Joseph, Soft Matter **8**, 10738 (2012).

[15] M. A. Alibakhshi, Q. Xie, Y. Li, and C. Duan, Scientific Reports **6**, 24936 (2016).

[16] M. Neek-Amal, A. Lohrasebi, M. Mousaei, F. Shayeganfar, B. Radha, and F. M. Peeters, Applied Physics Letters **113**, 083101 (2018).

[17] W.-J. Plug and J. Bruining, Advances in Water Resources **30**, 2339 (2007).

[18] J. Cai, T. Jin, J. Kou, S. Zou, J. Xiao, and Q. Meng, Langmuir **37**, 1623 (2021).

[19] S. K. Kannam, B. Todd, J. S. Hansen, and P. J. Daivis, The Journal of Chemical Physics **138** (2013).

[20] S. Gravelle, C. Ybert, L. Bocquet, and L. Joly, Physical Review E **93**, 033123 (2016).

[21] S. K. Kannam, B. Todd, J. S. Hansen, and P. J. Daivis, The Journal of Chemical Physics **135**, 144701 (2011).

[22] M. Neek-Amal, F. M. Peeters, I. V. Grigorieva, and A. K. Geim, ACS Nano **10**, 3685 (2016).

[23] S. Plimpton, Journal of Computational Physics **117**, 1 (1995).

[24] A. P. Thompson, H. M. Aktulga, R. Berger, D. S. Bolintineanu, W. M. Brown, P. S. Crozier, P. J. in't Veld, A. Kohlmeyer, S. G. Moore, T. D. Nguyen, *et al.*, Computer Physics Communications **271**, 108171 (2022).

[25] A. Hagler, E. Huler, and S. Lifson, Journal of the American Chemical Society **96**, 5319 (1974).

[26] C. Bosanquet, The London, Edinburgh, and Dublin Philosophical Magazine and Journal of Science **45**, 525 (1923).

[27] G. Martic, F. Gentner, D. Seveno, D. Coulon, J. De Coninck, and T. Blake, Langmuir **18**, 7971 (2002).

[28] R. Zhou, Z. Qiu, C. Sun, and B. Bai, Physics of Fluids **35**, 042005 (2023).

[29] M. Heiranian and N. R. Aluru, Physical Review E **105**, 055105 (2022).

[30] E. Oyarzua, J. H. Walther, A. Mejía, and H. A. Zambrano, Physical Chemistry Chemical Physics **17**, 14731 (2015).

[31] R. Major, J. Houston, M. McGrath, J. Siepmann, and X.-Y. Zhu, Physical Review Letters **96**, 177803 (2006).

[32] L. Fu, S. Merabia, and L. Joly, Physical Review Letters **119**, 214501 (2017).

[33] Y. Xie, L. Fu, T. Niehaus, and L. Joly, Physical Review Letters **125**, 014501 (2020).

[34] D. Schebarchov and S. Hendy, Physical Review E **78**, 046309 (2008).

[35] D. Dimitrov, A. Milchev, and K. Binder, Physical Review Letters **99**, 054501 (2007).

[36] M. E. Suk and N. R. Aluru, Nanoscale and Microscale Thermophysical Engineering **21**, 247 (2017).

[37] S. B. Lunowa, A. Mascini, C. Bringedal, T. Bultreys, V. Cnudde, and I. S. Pop, Langmuir **38**, 1680 (2022).

[38] A. Sam, R. Hartkamp, S. Kumar Kannam, J. S. Babu, S. P. Sathian, P. J. Daivis, and B. Todd, Molecular Simulation **47**, 905 (2021).

[39] M. Heiranian and N. R. Aluru, ACS Nano **14**, 272 (2019).

[40] D.-C. Yang, R. J. Castellano, R. P. Silvy, S. K. Lageshetty, R. F. Praino, F. Fornasiero, and J. W. Shan, Nano Letters (2023).

[41] X. Qin, Q. Yuan, Y. Zhao, S. Xie, and Z. Liu, Nano Letters **11**, 2173 (2011).